iScience

CellPress
OPEN ACCESS

Article

Interacting ventral temporal gradients of timescales and functional connectivity and their relationships to visual behavior

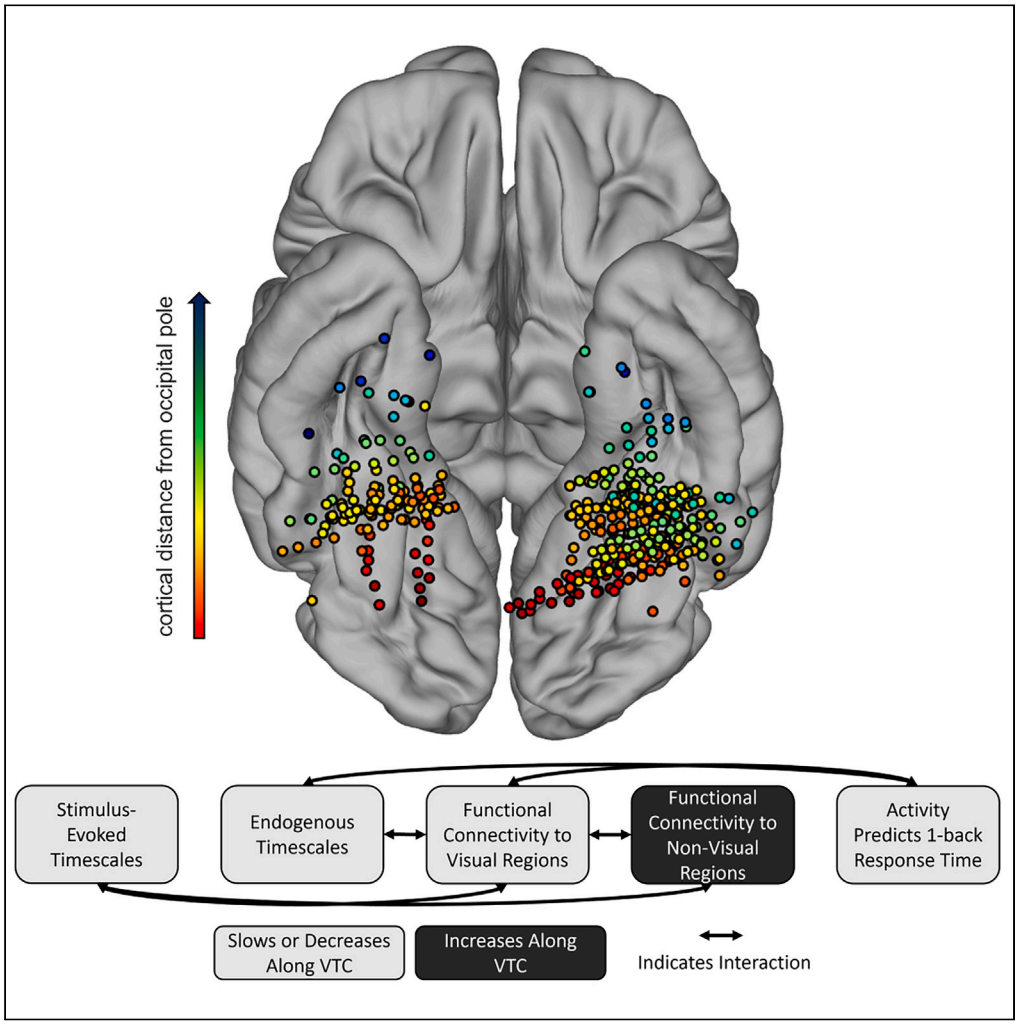

Matthew J. Boring, R. Mark Richardson, Avniel Singh Ghuman

ghumana@upmc.edu

Highlights

Neural timescales slow from posterior to anterior ventral temporal cortex

Stimulus-evoked and endogenous timescale do not correlate beyond shared anatomic axes

Functional connectivity and endogenous neural timescale gradients interact

Endogenous timescale and functional connectivity were related to visual reaction times

Boring et al., iScience 27, 110003
June 21, 2024 © 2024 Published by Elsevier Inc.
https://doi.org/10.1016/j.isci.2024.110003

iScience

CellPress
OPEN ACCESS

Article

Interacting ventral temporal gradients of timescales and functional connectivity and their relationships to visual behavior

Matthew J. Boring,[1,2,3] R. Mark Richardson,[3,4,5] and Avniel Singh Ghuman[1,2,3,6,*]

SUMMARY

Cortical gradients in endogenous and stimulus-evoked neurodynamic timescales, and long-range cortical interactions, provide organizational constraints to the brain and influence neural populations' roles in cognition. It is unclear how these functional gradients interrelate and which influence behavior. Here, intracranial recordings from 4,090 electrode contacts in 35 individuals map gradients of neural timescales and functional connectivity to assess their interactions along category-selective ventral temporal cortex. Endogenous and stimulus-evoked information processing timescales were not significantly correlated with one another suggesting that local neural timescales are context dependent and may arise through distinct neurophysiological mechanisms. Endogenous neural timescales correlated with functional connectivity even after removing the effects of shared anatomical gradients. Neural timescales and functional connectivity correlated with how strongly a population's activity predicted behavior in a simple visual task. These results suggest both interrelated and distinct neurophysiological processes give rise to different functional connectivity and neural timescale gradients, which together influence behavior.

INTRODUCTION

A neural population's functional properties, including its dynamics and its functional connectivity to other brain regions, are ultimately linked to that population's role in cognition and perception. Several gradients in functional properties have been shown to exist along the cortical axis spanning from primary sensory/motor areas to association cortices.[1–6] These gradients are thought to be related to key organizing principles of the cortex, guiding how different regions contribute to cognition and perception.[3,4,7,8] For example, there are gradients in the timescales over which neural populations accumulate information and endogenously fluctuate along this axis, with longer timescales further along cortical hierarchies,[5–7,9–13] though it remains unclear if stimulus processing and endogenous timescales are related to one another. Gradients of functional connectivity are also seen along this axis, with decreasing unimodal connectivity and increasing transmodal connectivity along cortical hierarchies.[3,14] These network-level neural properties likely influence local timescales, other computational characteristics of neural populations, and these populations' relationship to behavior.[2–4,15] However, empirical evidence linking functional gradients in local dynamics with gradients in the long-range connectivity of neural populations is limited. Additionally, it is uncertain to what degree these gradients relate to a neural population's role in behavior.

One prevalent functional gradient in cortex is the increasing timescales over which neural populations integrate information when moving from primary sensory/motor to association cortices.[5,6,9–11,16–18] For example, rapidly varying acoustic inputs represented in low-level auditory cortex are combined into more complex representations in higher-order auditory cortex, which operates over longer timescales.[12] These neural timescales, or temporal receptive windows, are related to the rate of decay of neural activity[9–11,16] because longer decay rates allow for more pieces of information to be integrated into a single representation. Stimulus-unrelated, endogenous timescales also lengthen along this axis, measured through the temporal autocorrelation of neural activity.[4,5,7,9,19] Variation in endogenous neural timescales has been shown to correlate with states of consciousness, self-consciousness, and neurological disorders like autism and schizophrenia.[7] It is unclear the extent to which stimulus-related and endogenous timescales relate to one another.

Another key aspect of neural dynamics, which is less well understood, is information processing dynamics, including the initial rate at which neural populations discriminate between stimuli (i.e., the duration of the initial rise of discriminant information in neural activity). Most previous studies have examined timescales of neural activity rather than discriminant information dynamics and have emphasized decay

[1]Center for Neuroscience at the University of Pittsburgh, University of Pittsburgh, Pittsburgh, PA, USA
[2]Center for the Neural Basis of Cognition, University of Pittsburgh and Carnegie Mellon University, Pittsburgh, PA, USA
[3]Department of Neurological Surgery, University of Pittsburgh, Pittsburgh, PA, USA
[4]Department of Neurosurgery, Massachusetts General Hospital, Boston, MA, USA
[5]Harvard Medical School, Boston, MA, USA
[6]Lead contact
*Correspondence: ghumana@upmc.edu
https://doi.org/10.1016/j.isci.2024.110003

durations, rather than rise duration.[9–11,16] The information processing dynamics during the initial rise relate to the speed of cortical computation and thus ultimately limit the speed of decision and action processes.[20] Despite the importance of a neural population's information processing dynamics in cognition and perception, the functional characteristics that are associated with neural populations that process information more quickly or slowly remain unclear.[10,11,17]

In addition to anatomical gradients in local neural dynamics, opposing anatomical gradients in long-distance connectivity to association versus primary sensory/motor cortices have also been demonstrated in human cortex. Unimodal connectivity, primarily within sensorimotor regions, decreases when moving up cortical processing hierarchies while transmodal connectivity linking multiple sensory domains increases.[1,3] However, it is unclear how gradients in local dynamics interact with gradients in long-range functional connectivity. *In silica*, circuit models of cortical processing suggest that inter- and intra-areal connectivity patterns help constrain a neural population's timescale,[2,8,21] which has received some support from low temporal resolution measures of brain activity.[15,22]

Finally, the functional properties that constrain a neural population's dynamics and long-range cortical connectivity ultimately constrain how that population contributes to cognition and perception. However, the specific aspects of a neural population's anatomical position, neurodynamics, and functional connectivity that are related to its ability to predict behavior have not been fully elucidated.

In the current study, category-selective neural populations in ventral temporal cortex (VTC) were used as a model to examine the relationship between anatomical gradients in local cortical processing and long-range cortical interactions. Focusing specifically on the ventral visual system allowed us to examine relationships between neural dynamics, stimulus information processing, and participant behavior more precisely than if we considered neural populations throughout cortex. This is because neural populations throughout cortex have varied relationships to perception and cognition, which limits our ability to examine information processing and behavior without investigating an exhaustive battery of tasks. Restricting our analysis allowed us to examine the time course of visual category-discriminant neural activity (which is primarily restricted to VTC) and separately analyze the effects of connectivity between category-discriminant populations and other visually responsive populations versus populations that were not visually responsive. Furthermore, this restriction allowed us to examine how the activity in category-selective populations correlated with participant response times (RTs) during a visual 1-back task. Thus, centering this study on category-selective neural populations in VTC allows us to ask fine-grained questions about information processing dynamics, functional connectivity patterns, and behavior. The caveat is that this choice leaves the generalizability of our findings to other sensory-motor and cognitive domains for future studies.

In addition, we explored endogenous timescales (i.e., neural dynamics not directly in response to the exogenous, stimulus-evoked activity) along VTC. Finally, we examine how these metrics of long-range cortical connectivity, neural dynamics, and correlates between neural activity and behavior interact with each other beyond any shared anatomical gradients.

RESULTS

Activity was recorded from 1,955 VTC electrode contacts (out of a total of 4,090 intracranial electrode contacts distributed throughout the brain) in 35 patients with pharmacologically intractable epilepsy (Figure S1) as they viewed images of objects (face, body, word, hammer, house, or phase-scrambled image) during a 1-back task. Multivariate Naive Bayes classifiers were used to predict the category of object participants were viewing during individual trials of the task using sliding 100 ms windows of single-trial potentials (stPs) and single-trial high-frequency broadband (stHFBB) activity recorded from individual electrode contacts. At this stage of the analysis, these signal components were combined since previous studies have suggested that they contain complementary information,[23] though in additional analyses they were examined separately.

Out of the 1,955 VTC electrode contacts, activity recorded from 390 electrode contacts (mean = 11; SD = 14 electrode contacts per patient) could reliably predict ($p < 0.001$, corrected via permutation testing) which category participants were viewing during single trials of the task (Figure 1). Information processing dynamics were estimated from the activity of the neural populations recorded by these contacts. Specifically, the time course of category-discriminant information processing in these category-discriminant neural populations was calculated by computing the mutual information (in bits) between the classifier outputs and the true category labels. The functional properties of these populations were computed to examine the relationship between these variables and anatomical axes of VTC (see STAR Methods). We examined gradients of, and interactions between, nine factors: two stimulus response timescales (initial rise duration and maintenance of category-discriminant information; factors 1 and 2; see Figure 2A for illustration); category-discriminant information onset time and peak magnitude (factors 3 and 4, see Figure 2A for illustration); two endogenous (prestimulus) timescales (factors 5 and 6), the timescale of decay, "tau," for the prestimulus stP and stHFBB autocorrelation functions (see Figure 3A for illustration); functional connectivity to visually responsive populations and to populations that were not significantly visually responsive (factors 7 and 8); and the accuracy of a neural population's activity for predicting behavioral RT (factor 9). We first examine these gradients individually to compare the results from human intracranial electroencephalography (iEEG) to prior results seen in other modalities[7] before examining their relationship to behavior and interactions among the factors.

Gradients of information processing dynamics

The cortical distance from the occipital pole, which roughly corresponds to the fovea in primary visual cortex, was used to approximate the position of neural populations along the hierarchical axis of the ventral visual stream.[24] Distance along this axis was correlated with several aspects of information processing in these category-discriminant neural populations (factors 1–4, Figure 2; see Figure S2 for an example from a single subject). Along this axis, neural populations demonstrated increasing onset latencies and increasing durations between this onset

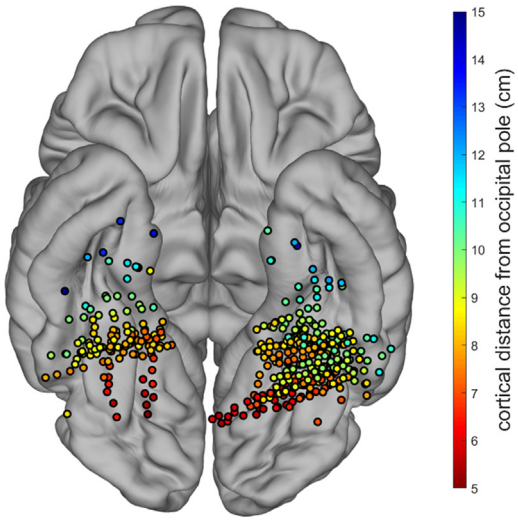

Figure 1. Category-selective VTC electrode contacts

Spatial topography of electrode contacts recording from neural populations that achieved peak category-discriminant information greater than chance at the $p < 0.001$ level corrected for multiple temporal comparisons. Colors represent the electrode contact's cortical distance from the occipital pole calculated using subject-specific anatomy. Depth electrode contacts are plotted below the cortical surface for clarity. Contacts that appeared to be outside of the Montreal Neurological Institute (MNI) standard brain due to differences in individual brain sizes were projected to the nearest MNI cortical vertex in this figure solely for illustrative purposes. The proportion of left versus right hemisphere category-discriminant contacts was comparable to the proportion of total left versus right hemisphere VTC implants (Figure S1).

and their peak time of category-discriminant information (see STAR Methods section "Neural information processing dynamics"). Additionally, neural populations maintained category-discriminant information longer after peaking, despite reaching smaller peak magnitudes, when moving along the visual hierarchy. Lengthening of these neural timescales along the visual hierarchy is generally consistent with prior studies.[9–11,16] However, the duration between onset and peak time (rise duration) has not generally been examined and the magnitude of the lengthening of this factor is greater than expected from visual models that assert that the dynamics should be governed primarily by conduction delays.[20,25] See Figure S3 for simulations demonstrating the independence of peak magnitude and rise duration metrics.

Gradients in information processing dynamics were present in individual patients (Figure S2), and several generalized across patients (linear mixed-effects models, Figure 2 caption). Notably, there were differences in these dynamic gradients when examining category-discriminant versus category-indiscriminant visual responsiveness in the same neural populations (Figure S4). Additionally, there were differences in these gradients across neural populations selective for different object categories, with face-selective populations generally displaying shallower posterior-anterior gradients than other category-selective populations (Figure S5; Table S1).

Gradients of endogenous neural timescales

Next, the endogenous neural timescales of VTC populations were quantified by computing the autocorrelation of prestimulus activity at multiple temporal lags and modeling the resulting autocorrelation curve with an exponential decay function[9,26] (factors 5–6, Figure 3, see STAR Methods section "Endogenous neural timescales"). When moving along the visual hierarchy, neural populations demonstrated increasing time constants of decay (tau) in the autocorrelation function of their prestimulus stP, indicating that their activity exhibited longer timescales/slower dynamics along this axis. This is consistent with previous studies observing slower endogenous timescales when moving up sensory processing hierarchies.[3,4,9,16,17,27]

Conversely, contrary to previous work that has only shown longer timescales along sensory processing hierarchies,[5–7,12,13] neural populations demonstrated shorter timescales in their prestimulus stHFBB activity when moving along the ventral visual hierarchy. Time constants across stP and stHFBB signal components were not significantly correlated with one another across electrode contacts ($\rho(390) = -0.05$, $p = 0.33$), highlighting the differentiability of these two aspects of the neural signal.[28–30] These results show that these components of the endogenous neural activity demonstrate distinct timescales that have opposite gradients along the ventral visual hierarchy.

Gradients in endogenous neural timescales were present in individual patients (Figure S2), and several generalized across patients (linear mixed-effects models, Figure 3 caption). Given the differences in endogenous neural timescales exhibited in stP and stHFBB, we recomputed gradients in information processing dynamics (factors 1–4) from these signal components separately. With a few notable exceptions, stimulus-related information processing dynamics demonstrated similar gradients for stP and stHFBB across these components when moving along the visual hierarchy (Figure S6).

Gradients of functional connectivity

After examining gradients in information processing and endogenous timescales, we examined gradients in functional connectivity along the ventral visual hierarchy. Specifically, a measure of functional connectedness to the rest of the brain, the average prestimulus phase-locking value (PLV), was calculated between the 390 category-discriminant VTC electrode contacts and all other electrode contacts implanted within the same patient (on average 115 electrode contacts, SD = 41). These "other" electrode contacts were located across the entire brain, not only in VTC (Figure S1). Here we report the metrics obtained when looking at functional connectivity from −450 to 0 ms before stimulus onset, but

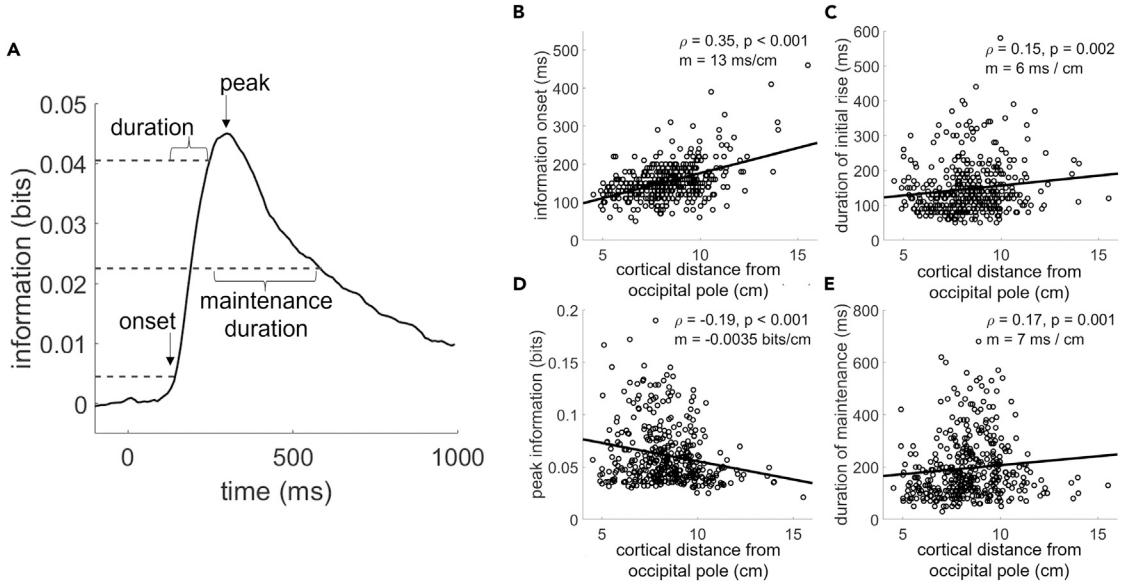

Figure 2. Category-discriminant information processing gradients along the ventral visual hierarchy

(A) The time course of category-discriminant information processing was computed for each neural population. The average time course across category-discriminant VTC populations is illustrated here. From each neural population's information processing time course, the information onset time (panel B), processing duration (C), peak magnitude (D), and maintenance duration (E) were computed. Simulations confirmed that decreases in information amplitude and information processing duration are independent using our methods (Figure S3). (B) The onset of category-discriminant information, defined as the time point the information reached 10% of the maximum before peaking, was significantly correlated with the position of that neural population along the ventral visual hierarchy. The black line indicates the least-squares regression fit. Spearman's ρ and associated p value shown on top right (n = 390). Spearman correlation was used because it is both more robust to outliers relative to Pearson's and is sensitive to non-linear monotonic relationships between variables, though this also means that the line drawn is not representative of the ρ. Slope of the least-squares regression line (m) indicated a 13 ms per centimeter increase in onset latency moving along VTC. Information onset was significantly associated with distance along the visual hierarchy even after correcting for cross-patient differences in onset latency (T(388) = 7.20, $p < 0.001$, tied-rank mixed-effects model). (C) The duration of the initial rise in category-discriminant information, defined as the time between the onset of information and the time it took the population to reach 90% of its peak information, was negatively correlated with distance along the visual hierarchy. The 90% threshold is used for the peak time because it better captures the initial rise in cases where there is a shallow peak among an extended plateau in the discriminant information time course. *Note*: All correlations remain significant across a substantial range of the heuristic thresholds chosen to define them (Figure S8), thus the selection of 10% and 90% as thresholds for onset and peak time do not drive these effects. The slope of the least-squares regression line indicated a 6 ms increase in the duration of the initial rise of information per cm of VTC. This relationship did not reach $p < 0.05$ when correcting for random cross-patient effects (T(388) = 1.55, p = 0.12, tied-rank mixed-effects model). (D) Peak category-discriminant information was negatively correlated with distance along the visual hierarchy, with a decrease of −0.0035 bits/cm. This relationship did not reach $p < 0.05$ when correcting for random cross-patient effects (T(388) = −1.62, p = 0.11, tied-rank mixed-effects model). There was a significant interaction between gender and distance along the visual hierarchy on peak category-discriminant information (T(386) = 3.24, p = 0.0013), with females having a stronger decrease compared to males. (E) Information maintenance duration, defined as the time between when the information first reached 90% and the time when it first decayed to 50% of the peak, was positively correlated with distance along the visual hierarchy. The slope of the least-squares regression line indicated a 7 ms increase in the duration of maintenance of information per cm of VTC. This relationship trended to $p < 0.05$ significance when correcting for random cross-patient effects (T(388) = 1.87, p = 0.063, tied-rank mixed-effects model).

none of the reported results changed substantially when looking at post-stimulus (50 to 450 ms) functional connectivity instead, since prestimulus and poststimulus connectivity were highly correlated (ρ(390) = 0.96, $p < 0.001$). Previous fMRI studies suggest opposite gradients in functional connectivity to unimodal sensory versus association and transmodal areas when moving along sensory processing streams.[1,3] Therefore, we separately computed the functional connectivity of VTC category-selective contacts to visually responsive contacts ($p < 0.001$, for visual stimulus response versus baseline, corrected for multiple temporal comparisons) and to those that were not visually responsive (factors 7–8, see STAR Methods section "Functional connectivity" for more methodological details). Also, given the wide variability of electrode coverage across patients, pooling connectivity across visually responsive and not-visually responsive contacts allowed us to partially overcome this cross-patient anatomical heterogeneity.

Connectivity between VTC electrode contacts and visually responsive contacts decreased when moving up the visual hierarchy. In contrast, the connectivity between VTC contacts and contacts that were not significantly visually responsive increased when moving up the visual hierarchy (Figure 4). Decreasing functional connectivity to visually responsive regions and increasing functional connectivity to regions that do not demonstrate strong visual responses are generally consistent with previous fMRI studies showing opposing anatomical gradients along VTC for functional connectivity to unimodal versus transmodal regions.[3]

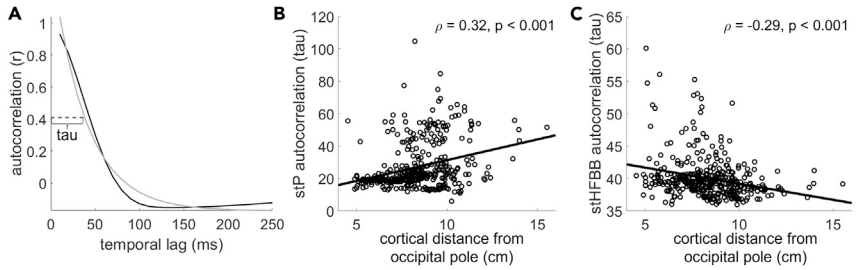

Figure 3. Prestimulus neural timescales along the ventral visual hierarchy

(A) For each neural population, the autocorrelation function during the −500 to 0 ms prestimulus period was computed for temporal lags ranging from 1 to 250 ms, averaged across trials (black line is the average across category-discriminant neural populations), and fit with a single exponential decay function (gray line). The timescale (tau) indicates how fast the fitted exponential function decays (dashed line; computed like those in[9]) and was correlated with other functional properties of the category-discriminant neural populations' activity.

(B) The autocorrelation function of single-trial potentials (stP) decayed more slowly when moving up the visual hierarchy, indicating that stP in more anterior VTC had higher autocorrelations at greater lags (longer timescales) relative to more posterior neural populations. This relationship held when correcting for random cross-patient effects ($T(388) = 8.03$, $p < 0.001$, tied-rank mixed-effects model).

(C) The autocorrelation function of single trial high frequency broadband (stHFBB) decayed more quickly when moving up the visual hierarchy, indicating that stHFBB in more anterior VTC had lower autocorrelations at greater lags (shorter timescales) relative to more posterior neural populations. This relationship also held when correcting for random cross-patient effects ($T(388) = -5.32$, $p < 0.001$, tied-rank mixed-effects model).

Gradients of ability to predict behavior

Additionally, we examined whether a neural population's role in visual perceptual behavior exhibited an anatomical gradient (factor 9). This was done by predicting the RT of patients, using sliding windows of neural activity recorded at each category-selective VTC electrode contact, during trials of the 1-back task where patients correctly responded that an object was presented twice in a row. How predictive the activity in an electrode contact was of RT was used as a measure of how much the activity from that neural population contributed to perceptual behavior (see STAR Methods section "Predicting response time from VTC activity"). When considering stP and stHFBB together, the ability of a VTC neural population's activity to predict RT was not significantly correlated with distance along the visual hierarchy ($\rho(390) = 0.02$, $p = 0.75$). However, when considering them separately, a neural population's ability to predict RT decreased along the visual hierarchy when looking at stHFBB but increased when looking at stP. These differences again highlight nuances in large-scale neuroanatomical gradients when considering different aspects of the neural signal.[28–30]

Relationships between and among neurodynamics, functional connectivity, and behavior

Given corresponding anatomical gradients in local dynamics and long-range cortical interactions, a key question is, to what degree these gradients interrelate beyond shared anatomical axes. To explore this question, the partial correlations between these functional properties of category-selective VTC populations were calculated after removing the effects of distance along the visual hierarchy (Figure 5). Spearman's partial correlation was used to remove any monotonic relationship to distance along the visual hierarchy; thus our analyses examined both linear and non-linear monotonic relationships (see Figure S7 for the non-partialed correlations and STAR Methods section "Quantification and statistical analysis" for further details).

The negative partial correlation between a neural population's stP timescale and its functional connectivity to visually responsive populations throughout the brain was significant. This suggests that parts of VTC that communicate strongly with other visually responsive regions have shorter timescales. Furthermore, the negative partial correlations were significant between the magnitude of a neural population's peak category-discriminant information and its connectivity to both visually responsive regions and regions that were not. This shows that neural populations with stronger connectivity, especially to non-visual areas, have less category-discriminant activity.

None of the measures of endogenous or stimulus-related information processing timescale (prestimulus stP and stHFBB tau, initial rise duration, and maintenance) were significantly correlated with one another, with or without removing the effects of distance along the visual hierarchy (Figures 5 and S7). Thus, though there are gradients in neural timescales across VTC using each of these measures, neither these timescales nor their gradients are significantly correlated to one another even though they were measured from the same neural populations. Notably though, endogenous autocorrelation timescales were correlated with poststimulus autocorrelation timescales calculated from 0 to 500 ms after stimulus onset (stP: $\rho(390) = 0.73$, $p < 0.001$ and stHFBB: $\rho(390) = 0.49$, $p < 0.001$), just not discriminant information processing dynamics. This suggests that neural timescales are context dependent (prestimulus- versus stimulus-related information processing, initial rise duration versus maintenance, stP versus stHFBB, etc. are all not significantly correlated) and measuring one type of timescale cannot be used to infer the general timescale of a neural population.

Partial correlations between nearly all the stimulus response variables (peak information, onset time, initial rise duration, and maintenance duration), other than the timescales noted in the prior paragraph (e.g., initial rise duration versus maintenance duration), were significantly correlated with one another. This suggests that there are interactive factors driving these different aspects of the stimulus response.

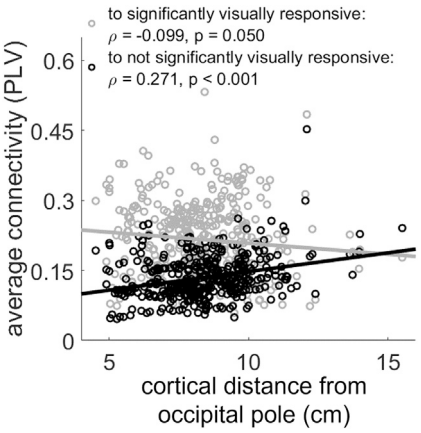

Figure 4. Gradients in long-range cortical interactions along the ventral visual hierarchy

The change in connectivity to visually responsive regions moving along VTC was opposite of the change in connectivity to populations that were not visually responsive. Connectivity to significantly visually responsive regions decreased along this axis, even when accounting for random cross-patient effects ($T(388) = -4.42$, $p < 0.001$, tied-rank mixed-effects model). On the other hand, connectivity to regions that were not significantly visually responsive increased along this axis, even when accounting for random cross-patient effects ($T(388) = 3.98$, $p < 0.001$, tied-rank mixed-effects model). There was a significant interaction between gender and distance along the visual hierarchy on connectivity to visual cortex ($T(386) = -3.19$, $p = 0.0016$, tied-rank mixed-effects model), with males having a stronger decrease along this axis.

The partial correlation between the ability of a neural population to predict RT and that neural population's connectivity to visually responsive brain regions and the partial correlation between a neural population's ability to predict RT and that neural population's prestimulus stP timescale after removing the effect of distance along the visual hierarchy were both significant (Figure 5). Thus, neural populations which integrate information over visual brain regions with short stP timescales were more predictive of behavior during the 1-back task observed here. This demonstrates that aspects of both local neural dynamics and long-range cortical interactions are intimately linked to a neural population's role in visual perceptual behavior.

DISCUSSION

Taken together, these results illustrate interrelationships between a neural population's anatomical location, its local dynamics, and its long-range functional connectivity, which ultimately influence that population's role in perception. Progressing along the ventral visual hierarchy was associated with decreases in peak category-discriminant information, longer information onsets, longer durations of initial information processing, longer periods of information maintenance, longer prestimulus stP timescales but shorter prestimulus stHFBB timescales, and opposing changes in connectivity to visual and non-visual brain regions. These results suggest that the anatomical and physiological gradients that exist along the visual hierarchy influence almost all of the examined aspects of prestimulus and information processing dynamics, which may constrain how these neural populations process information and their computational role in cognition. Indeed, a subset of these functional gradients was correlated with the ability of a neural population's activity to predict the speed of behavioral responses during a visual 1-back task. Furthermore, many aspects of stimulus response dynamics significantly related to one another beyond any shared relationship with anatomical location. Functional connectivity was correlated with aspects of both the stimulus response and prestimulus timescales, demonstrating how long-distance interactions can influence local neurodynamics. However, endogenous prestimulus timescales and post-stimulus information processing timescales were not strongly correlated to one another, nor were the initial rise and maintenance of the visual response, suggesting that neural timescales are context dependent and different aspects of neural dynamics arise through different processes and mechanisms.

Previous studies have observed that neural populations demonstrate longer timescales when moving from primary sensory and motor regions to association cortices.[5,6,9–11,16,17] The increasing endogenous timescales of stP activity along the ventral visual hierarchy observed here further support this organizing principle of cortex. Notably though, the endogenous stHFBB timescales demonstrated the opposite relationship along VTC, with shorter timescales in more anterior parts of VTC. Furthermore, the timescales of the stP and stHFBB were uncorrelated, demonstrating a dissociation between the dynamics of these two signal components recorded from the same neural population. Prior results show that different aspects of the iEEG signal arise from different cortical lamina and suggest that they may differentially reflect feedforward, feedback, and intra-areal communication.[29,31–33] The results here provide a hint of differences between the correlation of endogenous stP and stHFBB with functional connectivity between visually responsive versus non-visually responsive regions, though more so in the non-partial correlation matrix (Figure S7) than the partial correlation matrix (Figure 5). More broadly, these opposite and uncorrelated gradients highlight a need to better understand the differences in the physiological origins of stP and stHFBB signal components.[28–30]

The duration that category-discriminant neural populations initially process category-selective information increased along the ventral visual hierarchy, which may be the result of increased computational demands involved in forming more complex and individuated representations in more anterior category-selective neural populations.[34–37] However, in traditional models of perception, neural units are passive visual feature detectors that either fire or do not depending on the presence or absence of their preferred features.[25] In these models, little difference should be seen in the speed that neural populations process information further downstream because these passive feature detectors, even if they are sensitive to complex features, should respond rapidly and automatically to the presence of that feature.[25] In this study, the duration of the initial rise in category-discriminant information increased along the hierarchy, which does not fit with these traditional models, despite the duration of the initial rise visual responses (all visual activity versus baseline) remaining constant along the hierarchy (Figure S4). These results support a model of ventral visual representations that evolve through time, with information processing dynamics

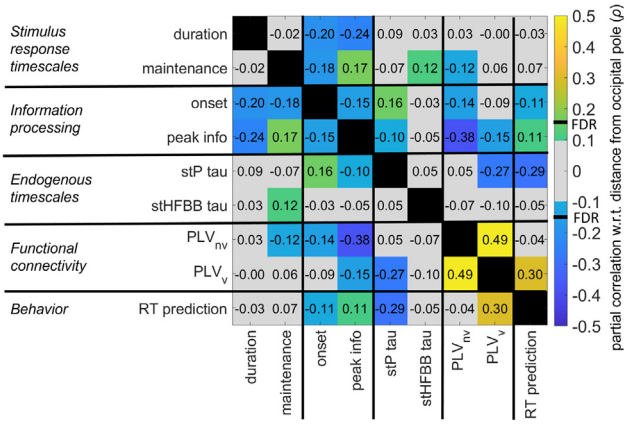

Figure 5. Interactions between local dynamics, long-range cortical interactions, and behavioral correlations

Partial correlation matrix between local dynamic properties and long-range cortical interactions after removing the effect of cortical distance along the visual hierarchy (see Figure S7 for non-partialed correlations). Colored squares are significant at the $p < 0.05$ level (uncorrected). The false discovery rate adjusted critical value corresponds to $\rho = \pm 0.146$. Within each square is the partial Spearman correlation coefficient for the variables in the corresponding row and column. The matrix is symmetric across the diagonal. Several properties of the local information processing dynamics, including information onset, peak magnitude, duration of the initial rise, and the amount of time the information was maintained, were significantly correlated to one another besides sharing a common anatomical gradient. The partial correlation between peak information and functional connectivity was also significant after removing the effect of distance along the visual hierarchy. The partial correlation between neural timescale (stP tau) and connectivity to visually responsive regions (PLV_v) was also significant as was the partial correlation between both connectivity to visual regions and stP timescale and a neural populations ability to predict patient response time (RT) during the 1-back task.

governed by interactions between the information being processed locally and globally through long-range connections, which reflect top-down and recurrent interactions.[38–41]

Long-range functional connectivity demonstrated a crossover effect along the ventral visual hierarchy, with decreasing connectivity to visually responsive regions and increasing connectivity to those that were not, consistent with previous fMRI studies.[1,3] Some of these gradients in functional connectivity were also associated with gradients in neural timescales even after controlling for effects of distance along the visual hierarchy. Specifically, neural populations that were more strongly connected to visually responsive regions demonstrated shorter endogenous stP timescales. One potential explanation for this result is that neural populations which integrate primarily visual inputs have faster timescales compared to neural populations that have more diverse inputs so that they are prepared to rapidly process incoming visual information.[3,11,24] Notably, the partial correlation between connectivity to regions that did not demonstrate strong visual responses and poststimulus stP timescale was not significant. Previous models have not investigated differential effects of long-range cortical interactions with visual versus non-visual regions on the timescale of neural populations.[8] This may be an important consideration for future models. Given the variable coverage of brain regions across patients in the current study, future studies are necessary to tease apart the impact that connectivity with specific brain regions has on local cortical dynamics.

Neural populations that demonstrated higher peak category-discriminant neural activity had earlier onsets and shorter durations of initial rise and maintained that information longer. Our simulations demonstrated that our measures of peak and duration are independent, confirming that this correlation is physiological and not an artifact of the analysis (Figure S3). Longer initial rises of category-discriminant information in neural populations with smaller peak information may reflect evidence accumulation over longer timescales in these populations.[11] Partial correlations between local neural dynamics and long-range cortical connectivity demonstrates that, in addition to sharing strong gradients along the primary axis of sensory processing systems, these properties of neural populations are closely linked to each other. These links between local dynamics and long-range cortical interactions are likely conferred in part by shared biochemical, microstructural, and macrostructural connectivity gradients that exist along the ventral visual axis beginning early in cortical development.[1–3,42,43]

Functional gradients in VTC were also correlated with the degree to which a neural population's activity could predict perceptual behavior. In the current study, increased functional connectivity to visually responsive regions and shorter prestimulus stP timescales were associated with a greater ability for a neural population's activity to predict RT in a 1-back task after removing the effect of distance along VTC. This suggests that these neural populations may play a larger role in the basic visual discrimination task studied here.

The "endogenous" activity studied here was taken from the prestimulus interval, during which participants were still engaged in the visual 1-back task, rather than true "resting-state" data. Therefore, anticipatory or other effects could potentially influence these results (e.g., while the activity is "endogenous" it may not be "spontaneous"). It is notable that these results cannot address relationships between neurodynamics and perception or behavior in other tasks. Behaviors involving more complex perceptual representations and/or more complex behavioral decisions may rely more heavily on neural populations with longer timescales and on higher-order cortical regions.[39,40,44–47] Future studies are required to determine if finer level visual discrimination involving longer RTs[48] reflects contributions from neural populations with different information processing timescales and functional connectivity patterns compared to those involved in the 1-back task studied here.

Furthermore, it may be interesting to determine if feedback and/or feedforward interactions differentially contribute to perceptual behaviors of different tasks.

There were not significant correlations between stimulus response timescales and endogenous timescales, or between onset dynamics and maintenance dynamics. Different aspects of task-evoked timescales were not closely linked to one another, suggesting the physiological drivers of initial information processing and maintenance may be independent. Additionally, endogenous neurodynamic timescales did not generalize to stimulus-related information processing timescales. Notably, this is unlike functional connectivity patterns, which were highly correlated across the stimulus response and prestimulus periods ($\rho > 0.95$). The lack of significant correlation across the different measures of local neurodynamics highlights that endogenous neural timescales are not necessarily tightly related to stimulus-evoked information processing dynamics after removing the effects of their shared gradients along cortical processing hierarchies.[13,49–51] Thus, inferences about a region's computational role in cognition, including its temporal integration and segregation[7] or temporal response windows,[16,27] cannot be inferred from endogenous dynamics alone, as stimulus information processing and endogenous timescales are not necessarily strongly correlated. There is no single principle or process that governs a neural population's timescales; e.g., timescales are not a static and inherent property of a neural population.[7,52] Rather, these results suggest that the anatomical differences in these types of timescales are governed by different combinations of factors that can depend on cognitive and neural context.[53] That said, there is increasing evidence that prestimulus activity can influence poststimulus activity on a trial-by-trial basis,[54–56] including a prior study from our group using a subset of the data presented here.[55] The results here do not contradict these prior observations, as this study examines anatomical differences in mean dynamics, not trial-by-trial relationships.

The current study highlights how large-scale anatomical and functional gradients interact to constrain local neural processing dynamics and computation. The anatomical gradients of dynamics and connectivity demonstrated here impose important constraints for future neurobiological models of visual perception. This architecture may help the brain achieve abstract and conceptual representations seen in more anterior VTC neural populations.[34,36,37] While the present study examined these effects in visual processing, it is likely that similar principles apply to other hierarchically organized sensory and cognitive systems.[3,10,12,52] However, more studies are necessary to confirm the observed principles in other sensory and cognitive processing hierarchies. Indeed, gradients in physiological, and thus functional, organization are likely in part conferred by corresponding gradients in growth factors and, in turn, gene expression during and persisting after cortical development.[3,4,42,43] Interactions among response properties and functional connectivity patterns of neural populations suggest that shared neurophysiological mechanisms tie large-scale and local processing dynamics together. Distinctions among and between endogenous and stimulus response timescales suggest that these neurodynamics are caused by distinct neurobiological mechanisms and play different roles in the brain. These results highlight the mutual interrelationships between a neural population's position in the processing hierarchy, its functional connectivity, and its local dynamics, constraining its role in cognition.

Limitations of the study

In this study, functional and anatomical gradients of visual information processing were examined with an emphasis on ventral visual cortex. Other studies are necessary to determine if the interactions observed here are comparable to those in other sensory or motor cortical systems. Additionally, in this study, prestimulus activity was used to approximate intrinsic neural dynamics. Therefore, we cannot rule out effects of anticipation or working memory in the endogenous neural timescales reported here.

STAR★METHODS

Detailed methods are provided in the online version of this paper and include the following:

- KEY RESOURCES TABLE
- RESOURCE AVAILABILITY
  - Lead contact
  - Materials availability
  - Data and code availability
- EXPERIMENTAL MODEL AND STUDY PARTICIPANT DETAILS
  - Intracranial electroencephalography patients
- METHOD DETAILS
  - Experimental paradigm
  - Intracranial recordings
  - Multivariate temporal pattern analysis
  - Neural information processing dynamics
  - Category-selective VTC electrode contacts
  - Information processing simulations
  - Endogenous neural timescales
  - Functional connectivity
  - Predicting response time from VTC activity
- QUANTIFICATION AND STATISTICAL ANALYSIS

SUPPLEMENTAL INFORMATION

Supplemental information can be found online at https://doi.org/10.1016/j.isci.2024.110003.

ACKNOWLEDGMENTS

The authors would like to thank the patients and staff in the University of Pittsburgh Comprehensive Epilepsy Center at the University of Pittsburgh Medical Center for their participation in this research study. They would also like to thank Marlene Behrmann, Michael Tarr, and Max G'Sell for helpful suggestions in the design of the experimental analyses in addition to Michael Ward, Shawn Walls, and Ashley C. Whiteman for their help with data collection. The authors gratefully acknowledge the funding support of the National Institute of Mental Health under R21EY030297, R01MH132225, and P50MH109429 National Science Foundation under 1734907, and National Institutes of Health under T32NS007433-20.

AUTHOR CONTRIBUTIONS

Conceptualization, M.J.B. and A.S.G.; methodology, M.J.B. and A.S.G.; investigation, M.J.B., R.M.R., and A.S.G.; formal analysis, M.J.B.; writing – original draft, M.J.B. and A.S.G.; writing – review & editing, M.J.B., R.M.R., and A.S.G.; resources, R.M.R. and A.S.G.; funding acquisition, A.S.G.

DECLARATION OF INTERESTS

The authors declare no competing interests.

Received: November 11, 2022
Revised: April 2, 2024
Accepted: May 14, 2024
Published: May 15, 2024

REFERENCES

1. Paquola, C., Vos De Wael, R., Wagstyl, K., Bethlehem, R.A.I., Hong, S.J., Seidlitz, J., Bullmore, E.T., Evans, A.C., Misic, B., Margulies, D.S., et al. (2019). Microstructural and functional gradients are increasingly dissociated in transmodal cortices. PLoS Biol. *17*, e3000284. https://doi.org/10.1371/journal.pbio.3000284.
2. Demirtaş, M., Burt, J.B., Helmer, M., Ji, J.L., Adkinson, B.D., Glasser, M.F., Van Essen, D.C., Sotiropoulos, S.N., Anticevic, A., and Murray, J.D. (2019). Hierarchical Heterogeneity across Human Cortex Shapes Large-Scale Neural Dynamics. Neuron *101*, 1181–1194.e13. https://doi.org/10.1016/j.neuron.2019.01.017.
3. Huntenburg, J.M., Bazin, P.L., and Margulies, D.S. (2018). Large-Scale Gradients in Human Cortical Organization. Trends Cogn. Sci. *22*, 21–31. https://doi.org/10.1016/j.tics.2017.11.002.
4. Gao, R., Van den Brink, R.L., Pfeffer, T., and Voytek, B. (2020). Neuronal timescales are functionally dynamic and shaped by cortical microarchitecture. Elife *9*, e61277. https://doi.org/10.7554/eLife.61277.
5. Shafiei, G., Markello, R.D., Vos de Wael, R., Bernhardt, B.C., Fulcher, B.D., and Misic, B. (2020). Topographic gradients of intrinsic dynamics across neocortex. Elife *9*, e62116. https://doi.org/10.7554/ELIFE.62116.
6. Mahjoory, K., Schoffelen, J.M., Keitel, A., and Gross, J. (2020). The frequency gradient of human resting-state brain oscillations follows cortical hierarchies. Elife *9*, e53715. https://doi.org/10.7554/ELIFE.53715.
7. Wolff, A., Berberian, N., Golesorkhi, M., Gomez-Pilar, J., Zilio, F., and Northoff, G. (2022). Intrinsic neural timescales: temporal integration and segregation. Trends Cogn. Sci. *26*, 159–173. https://doi.org/10.1016/j.tics.2021.11.007.
8. Chaudhuri, R., Knoblauch, K., Gariel, M.-A., Kennedy, H., and Wang, X.-J. (2015). A Large-Scale Circuit Mechanism for Hierarchical Dynamical Processing in the Primate Cortex. Neuron *88*, 419–431. https://doi.org/10.1016/J.NEURON.2015.09.008.
9. Murray, J.D., Bernacchia, A., Freedman, D.J., Romo, R., Wallis, J.D., Cai, X., Padoa-Schioppa, C., Pasternak, T., Seo, H., Lee, D., and Wang, X.J. (2014). A hierarchy of intrinsic timescales across primate cortex. Nat. Neurosci. *17*, 1661–1663. https://doi.org/10.1038/nn.3862.
10. Runyan, C.A., Piasini, E., Panzeri, S., and Harvey, C.D. (2017). Distinct timescales of population coding across cortex. Nature *548*, 92–96. https://doi.org/10.1038/nature23020.
11. Honey, C.J., Thesen, T., Donner, T.H., Silbert, L.J., Carlson, C.E., Devinsky, O., Doyle, W.K., Rubin, N., Heeger, D.J., and Hasson, U. (2012). Slow Cortical Dynamics and the Accumulation of Information over Long Timescales. Neuron *76*, 423–434. https://doi.org/10.1016/j.neuron.2012.08.011.
12. Ding, N., Melloni, L., Zhang, H., Tian, X., and Poeppel, D. (2016). Cortical tracking of hierarchical linguistic structures in connected speech. Nat. Neurosci. *19*, 158–164. https://doi.org/10.1038/nn.4186.
13. Spitmaan, M., Seo, H., Lee, D., and Soltani, A. (2020). Multiple timescales of neural dynamics and integration of task-relevant signals across cortex. Proc. Natl. Acad. Sci. USA *117*, 22522–22531. https://doi.org/10.1073/pnas.2005993117.
14. Margulies, D.S., Ghosh, S.S., Goulas, A., Falkiewicz, M., Huntenburg, J.M., Langs, G., Bezgin, G., Eickhoff, S.B., Castellanos, F.X., Petrides, M., et al. (2016). Situating the default-mode network along a principal gradient of macroscale cortical organization. Proc. Natl. Acad. Sci. USA *113*, 12574–12579. https://doi.org/10.1073/pnas.1608282113.
15. Ito, T., Hearne, L.J., and Cole, M.W. (2020). A cortical hierarchy of localized and distributed processes revealed via dissociation of task activations, connectivity changes, and intrinsic timescales. Neuroimage *221*, 117141. https://doi.org/10.1016/J.NEUROIMAGE.2020.117141.
16. Hasson, U., Yang, E., Vallines, I., Heeger, D.J., and Rubin, N. (2008). A Hierarchy of Temporal Receptive Windows in Human Cortex. J. Neurosci. *28*, 2539–2550. https://doi.org/10.1523/JNEUROSCI.5487-07.2008.
17. Kiebel, S.J., Daunizeau, J., and Friston, K.J. (2008). A hierarchy of time-scales and the brain. PLoS Comput. Biol. *4*, e1000209. https://doi.org/10.1371/journal.pcbi.1000209.
18. Cocchi, L., Sale, M.V., L Gollo, L., Bell, P.T., Nguyen, V.T., Zalesky, A., Breakspear, M., and Mattingley, J.B. (2016). A hierarchy of timescales explains distinct effects of local inhibition of primary visual cortex and frontal eye fields. Elife *5*, e15252. https://doi.org/10.7554/eLife.15252.
19. Raut, R.V., Snyder, A.Z., and Raichle, M.E. (2020). Hierarchical dynamics as a macroscopic organizing principle of the human brain. Proc. Natl. Acad. Sci. USA *117*, 20890–20897. https://doi.org/10.1073/pnas.2003383117.
20. Thorpe, S., Fize, D., and Marlot, C. (1996). Speed of processing in the human visual system. Nature *381*, 520–522. https://doi.org/10.1038/381520a0.
21. Kong, X., Kong, R., Orban, C., Wang, P., Zhang, S., Anderson, K., Holmes, A., Murray, J.D., Deco, G., van den Heuvel, M., and Yeo,

B.T.T. (2021). Sensory-motor cortices shape functional connectivity dynamics in the human brain. Nat. Commun. *12*, 6373. https://doi.org/10.1038/s41467-021-26704-y.

22. Manea, A.M.G., Zilverstand, A., Ugurbil, K., Heilbronner, S.R., and Zimmermann, J. (2022). Intrinsic timescales as an organizational principle of neural processing across the whole rhesus macaque brain. Elife *11*, e75540. https://doi.org/10.7554/ELIFE.75540.
23. Miller, K.J., Schalk, G., Hermes, D., Ojemann, J.G., and Rao, R.P.N. (2016). Spontaneous Decoding of the Timing and Content of Human Object Perception from Cortical Surface Recordings Reveals Complementary Information in the Event-Related Potential and Broadband Spectral Change. PLoS Comput. Biol. *12*, e1004660. https://doi.org/10.1371/journal.pcbi.1004660.
24. Kravitz, D.J., Saleem, K.S., Baker, C.I., Ungerleider, L.G., and Mishkin, M. (2013). The ventral visual pathway: an expanded neural framework for the processing of object quality. Trends Cogn. Sci. *17*, 26–49. https://doi.org/10.1016/j.tics.2012.10.011.
25. Serre, T., Oliva, A., and Poggio, T. (2007). A feedforward architecture accounts for rapid categorization. Proc. Natl. Acad. Sci. USA *104*, 6424–6429. https://doi.org/10.1073/pnas.0700622104.
26. Cavanagh, S.E., Wallis, J.D., Kennerley, S.W., and Hunt, L.T. (2016). Autocorrelation structure at rest predicts value correlates of single neurons during reward-guided choice. Elife *5*, e18937. https://doi.org/10.7554/eLife.18937.
27. Lerner, Y., Honey, C.J., Silbert, L.J., and Hasson, U. (2011). Topographic Mapping of a Hierarchy of Temporal Receptive Windows Using a Narrated Story. J. Neurosci. *31*, 2906–2915. https://doi.org/10.1523/JNEUROSCI.3684-10.2011.
28. Engell, A.D., and McCarthy, G. (2011). The relationship of gamma oscillations and face-specific ERPs recorded subdurally from occipitotemporal cortex. Cereb. Cortex *21*, 1213–1221. https://doi.org/10.1093/cercor/bhq206.
29. Leszczyński, M., Barczak, A., Kajikawa, Y., Ulbert, I., Falchier, A.Y., Tal, I., Haegens, S., Melloni, L., Knight, R.T., and Schroeder, C.E. (2020). Dissociation of broadband high-frequency activity and neuronal firing in the neocortex. Sci. Adv. *6*, eabb0977. https://doi.org/10.1126/sciadv.abb0977.
30. Boring, M.J., Silson, E.H., Ward, M.J., Richardson, R.M., Fiez, J.A., Baker, C.I., and Ghuman, A.S. (2021). Multiple adjoining word- and face-selective regions in ventral temporal cortex exhibit distinct dynamics. J. Neurosci. *41*, 6314–6327. https://doi.org/10.1523/JNEUROSCI.3234-20.2021.
31. Bastos, A.M., Vezoli, J., Bosman, C.A., Schoffelen, J.M., Oostenveld, R., Dowdall, J.R., DeWeerd, P., Kennedy, H., and Fries, P. (2015). Visual Areas Exert Feedforward and Feedback Influences through Distinct Frequency Channels. Neuron *85*, 390–401. https://doi.org/10.1016/J.NEURON.2014.12.018.
32. Van Kerkoerle, T., Self, M.W., Dagnino, B., Gariel-Mathis, M.A., Poort, J., Van Der Togt, C., and Roelfsema, P.R. (2014). Alpha and gamma oscillations characterize feedback and feedforward processing in monkey visual cortex. Proc. Natl. Acad. Sci. USA *111*, 14332–14341. https://doi.org/10.1073/PNAS.1402773111.
33. Buffalo, E.A., Fries, P., Landman, R., Buschman, T.J., and Desimone, R. (2011). Laminar differences in gamma and alpha coherence in the ventral stream. Proc. Natl. Acad. Sci. USA *108*, 11262–11267. https://doi.org/10.1073/PNAS.1011284108.
34. Freiwald, W.A., and Tsao, D.Y. (2010). Functional compartmentalization and viewpoint generalization within the macaque face-processing system. Science *330*, 845–851. https://doi.org/10.1126/science.1194908.
35. Vinckier, F., Dehaene, S., Jobert, A., Dubus, J.P., Sigman, M., and Cohen, L. (2007). Hierarchical Coding of Letter Strings in the Ventral Stream: Dissecting the Inner Organization of the Visual Word-Form System. Neuron *55*, 143–156. https://doi.org/10.1016/J.NEURON.2007.05.031.
36. Abel, T.J., Rhone, A.E., Nourski, K.V., Kawasaki, H., Oya, H., Griffiths, T.D., Howard, M.A., and Tranel, D. (2015). Direct physiologic evidence of a heteromodal convergence region for proper naming in human left anterior temporal lobe. J. Neurosci. *35*, 1513–1520. https://doi.org/10.1523/JNEUROSCI.3387-14.2015.
37. Clarke, A., Taylor, K.I., and Tyler, L.K. (2011). The Evolution of Meaning: Spatio-temporal Dynamics of Visual Object Recognition. J. Cogn. Neurosci. *23*, 1887–1899. https://doi.org/10.1162/jocn.2010.21544.
38. Sugase, Y., Yamane, S., Ueno, S., and Kawano, K. (1999). Global and fine information coded by single neurons in the temporal visual cortex. Nature *400*, 869–873. https://doi.org/10.1038/23703.
39. Ghuman, A.S., Brunet, N.M., Li, Y., Konecky, R.O., Pyles, J.A., Walls, S.A., Destefino, V., Wang, W., and Richardson, R.M. (2014). Dynamic encoding of face information in the human fusiform gyrus. Nat. Commun. *5*, 5672. https://doi.org/10.1038/ncomms6672.
40. Hirshorn, E.A., Li, Y., Ward, M.J., Richardson, R.M., Fiez, J.A., and Ghuman, A.S. (2016). Decoding and disrupting left midfusiform gyrus activity during word reading. Proc. Natl. Acad. Sci. USA *113*, 8162–8167. https://doi.org/10.1073/pnas.1604126113.
41. Koyano, K.W., Jones, A.P., McMahon, D.B.T., Waidmann, E.N., Russ, B.E., and Leopold, D.A. (2021). Dynamic Suppression of Average Facial Structure Shapes Neural Tuning in Three Macaque Face Patches. Curr. Biol. *31*, 1–12.e5. https://doi.org/10.1016/j.cub.2020.09.070.
42. Sansom, S.N., and Livesey, F.J. (2009). Gradients in the brain: the control of the development of form and function in the cerebral cortex. Cold Spring Harb. Perspect. Biol. *1*, a002519. https://doi.org/10.1101/cshperspect.a002519.
43. Burt, J.B., Demirtaş, M., Eckner, W.J., Navejar, N.M., Ji, J.L., Martin, W.J., Bernacchia, A., Anticevic, A., and Murray, J.D. (2018). Hierarchy of transcriptomic specialization across human cortex captured by structural neuroimaging topography. Nat. Neurosci. *21*, 1251–1259.
44. Ghuman, A.S., and Martin, A. (2019). Dynamic Neural Representations: An Inferential Challenge for fMRI. Trends Cogn. Sci. *23*, 534–536. https://doi.org/10.1016/j.tics.2019.04.004.
45. Li, Y., Richardson, R.M., and Ghuman, A.S. (2019). Posterior Fusiform and Midfusiform Contribute to Distinct Stages of Facial Expression Processing. Cereb. Cortex *29*, 3209–3219. https://doi.org/10.1093/cercor/bhy186.
46. Tang, H., Buia, C., Madhavan, R., Crone, N.E., Madsen, J.R., Anderson, W.S., and Kreiman, G. (2014). Spatiotemporal Dynamics Underlying Object Completion in Human Ventral Visual Cortex. Neuron *83*, 736–748. https://doi.org/10.1016/j.neuron.2014.06.017.
47. Quiroga, R.Q., Mukamel, R., Isham, E.A., Malach, R., and Fried, I. (2008). Human single-neuron responses at the threshold of conscious recognition. Proc. Natl. Acad. Sci. USA *105*, 3599–3604. https://doi.org/10.1073/pnas.0707043105.
48. Kampf, M., Nachson, I., and Babkoff, H. (2002). A serial test of the laterality of familiar face recognition. Brain Cogn. *50*, 35–50. https://doi.org/10.1016/S0278-2626(02)00008-8.
49. Mellem, M.S., Wohltjen, S., Gotts, S.J., Ghuman, A.S., and Martin, A. (2017). Intrinsic frequency biases and profiles across human cortex. J. Neurophysiol. *118*, 2853–2864. https://doi.org/10.1152/jn.00061.2017.
50. Ghuman, A.S., Van Den Honert, R.N., and Martin, A. (2013). Interregional neural synchrony has similar dynamics during spontaneous and stimulus-driven states. Sci. Rep. *3*, 1481. https://doi.org/10.1038/srep01481.
51. Churchland, M.M., Yu, B.M., Cunningham, J.P., Sugrue, L.P., Cohen, M.R., Corrado, G.S., Newsome, W.T., Clark, A.M., Hosseini, P., Scott, B.B., et al. (2010). Stimulus onset quenches neural variability: A widespread cortical phenomenon. Nat. Neurosci. *13*, 369–378. https://doi.org/10.1038/nn.2501.
52. Rossi-Pool, R., Zainos, A., Alvarez, M., Parra, S., Zizumbo, J., and Romo, R. (2021). Invariant timescale hierarchy across the cortical somatosensory network. Proc. Natl. Acad. Sci. USA *118*, e2021843118. https://doi.org/10.1073/PNAS.2021843118.
53. Golesorkhi, M., Gomez-Pilar, J., Tumati, S., Fraser, M., and Northoff, G. (2021). Temporal hierarchy of intrinsic neural timescales converges with spatial core-periphery organization. Commun. Biol. *4*, 277. https://doi.org/10.1038/s42003-021-01785-z.
54. He, B.J. (2013). Spontaneous and Task-Evoked Brain Activity Negatively Interact. J. Neurosci. *33*, 4672–4682. https://doi.org/10.1523/JNEUROSCI.2922-12.2013.
55. Li, Y., Ward, M.J., Richardson, R.M., G'Sell, M., and Ghuman, A.S. (2020). Endogenous activity modulates stimulus and circuit-specific neural tuning and predicts perceptual behavior. Nat. Commun. *111*, 4014. https://doi.org/10.1038/s41467-020-17729-w.
56. Braun, W., Matsuzaka, Y., Mushiake, H., Northoff, G., and Longtin, A. (2022). Non-additive activity modulation during a decision making task involving tactic selection. Cogn. Neurodyn. *16*, 117–133. https://doi.org/10.1007/S11571-021-09702-0.
57. Tadel, F., Baillet, S., Mosher, J.C., Pantazis, D., and Leahy, R.M. (2011). Brainstorm: a user-friendly application for MEG/EEG analysis. Comput. Intell. Neurosci. *2011*, 879716. https://doi.org/10.1155/2011/879716.
58. Dale, A.M., Fischl, B., and Sereno, M.I. (1999). Cortical Surface-Based Analysis. Neuroimage *9*, 179–194. https://doi.org/10.1006/nimg.1998.0395.
59. Hermes, D., Miller, K.J., Noordmans, H.J., Vansteensel, M.J., and Ramsey, N.F. (2010). Automated electrocorticographic electrode

localization on individually rendered brain surfaces. J. Neurosci. Methods *185*, 293–298. https://doi.org/10.1016/j.jneumeth.2009.10.005.

60. Evans, A.C., Collins, D.L., Mills, S.R., Brown, E.D., Kelly, R.L., and Peters, T.M. (1994). 3D statistical neuroanatomical models from 305 MRI volumes. In IEEE Nuclear Science Symposium & Medical Imaging Conference (IEEE), pp. 1813–1817. https://doi.org/10.1109/nssmic.1993.373602.
61. Kirsanov, D. (2021). Exact geodesic for triangular meshes, MATLAB Central File Exchange. Retrieved May 21, 2020. https://www.mathworks.com/matlabcentral/fileexchange/18168-exact-geodesic-for-triangular-meshes.
62. Brainard, D.H. (1997). The Psychophysics Toolbox. Spat. Vis. *10*, 433–436. https://doi.org/10.1163/156856897X00357.
63. Oostenveld, R., Fries, P., Maris, E., and Schoffelen, J.-M. (2011). FieldTrip: Open source software for advanced analysis of MEG, EEG, and invasive electrophysiological data. Comput. Intell. Neurosci. *2011*, 156869. https://doi.org/10.1155/2011/156869.
64. Miller, K.J. (2010). Broadband spectral change: Evidence for a macroscale correlate of population firing rate? J. Neurosci. *30*, 6477–6479. https://doi.org/10.1523/JNEUROSCI.6401-09.2010.
65. Crone, N.E., Sinai, A., and Korzeniewska, A. (2006). High-frequency gamma oscillations and human brain mapping with electrocorticography. Prog. Brain Res. *159*, 275–295. https://doi.org/10.1016/S0079-6123(06)59019-3.
66. Rolls, E.T., Treves, A., and Tovee, M.J. (1997). The representational capacity of the distributed encoding of information provided by populations of neurons in primate temporal visual cortex. Exp. Brain Res. *114*, 149–162. https://doi.org/10.1007/PL00005615.
67. Rolls, E.T., Critchley, H.D., and Treves, A. (1996). Representation of olfactory information in the primate orbitofrontal cortex. J. Neurophysiol. *75*, 1982–1996. https://doi.org/10.1152/jn.1996.75.5.1982.
68. Samengo, I. (2002). Information Loss in an Optimal Maximum Likelihood Decoding. Neural Comput. *14*, 771–779. https://doi.org/10.1162/089976602317318947.
69. Behrmann, M., and Plaut, D.C. (2013). Distributed circuits, not circumscribed centers, mediate visual recognition. Trends Cogn. Sci. *17*, 210–219. https://doi.org/10.1016/j.tics.2013.03.007.
70. Maris, E., and Oostenveld, R. (2007). Nonparametric statistical testing of EEG- and MEG-data. J. Neurosci. Methods *164*, 177–190. https://doi.org/10.1016/J.JNEUMETH.2007.03.024.
71. Lachaux, J.-P., Rodriguez, E., Martinerie, J., and Varela, F.J. (1999). Measuring Phase Synchrony in Brain Signals. Hum. Brain Mapp. *8*, 194–208.
72. Lowet, E., Roberts, M.J., Bonizzi, P., Karel, J., and De Weerd, P. (2016). Quantifying Neural Oscillatory Synchronization: A Comparison between Spectral Coherence and Phase-Locking Value Approaches. PLoS One *11*, e0146443. https://doi.org/10.1371/journal.pone.0146443.
73. Ghuman, A.S., McDaniel, J.R., and Martin, A. (2011). A wavelet-based method for measuring the oscillatory dynamics of resting-state functional connectivity in MEG. Neuroimage *56*, 69–77. https://doi.org/10.1016/j.neuroimage.2011.01.046.
74. Benjamini, Y., and Yekutieli, D. (2001). The control of the false discovery rate in multiple testing under dependency. Ann. Stat. *29*, 1165–1188. https://doi.org/10.1214/aos/1013699998.
75. Luke, S.G. (2017). Evaluating significance in linear mixed-effects models in R. Behav. Res. Methods *49*, 1494–1502. https://doi.org/10.3758/s13428-016-0809-y.

STAR★METHODS

KEY RESOURCES TABLE

REAGENT or RESOURCE	SOURCE	IDENTIFIER
Software and algorithms		
Matlab R2018b	Mathworks	SCR_001622
Psychophysics Toolbox	psychtoolbox.org	SCR_002881
FieldTrip Toolbox	fieldtriptoolbox.org	SCR_004849
Brainstorm Toolbox	neuroimage.usc.edu	SCR_001761
Freesurfer	surfer.nmr.mgh.harvard.edu	SCR_001847
Exact Geodesic for Triangular Meshes	https://www.mathworks.com/matlabcentral/fileexchange/18168-exact-geodesic-for-triangular-meshes	Version 1.0.0.0

RESOURCE AVAILABILITY

Lead contact

Requests for further information should be directed to Avniel Ghuman (ghumana@upmc.edu).

Materials availability

This study did not generate new unique reagents.

Data and code availability

- Anonymized intracranial EEG and structural MRI data will be made available on demand by the lead contact in compliance with restrictions imposed by the University of Pittsburgh IRB.
- This study did not report original code.
- Any additional information required to replicate the analyses reported in this paper is available from the lead contact upon request.

EXPERIMENTAL MODEL AND STUDY PARTICIPANT DETAILS

Intracranial electroencephalography patients

Stereotactic depth and surface electrocorticography (ECoG) electrodes were implanted in ventral temporal cortex (VTC) of 41 patients (15 males, 26 females; 3 Black, 38 White; ages 19-65) for the localization of pharmacologically intractable epileptiform activity. Different aspects of these recordings from 38 of these patients were previously reported.[30] All patients gave written informed consent under protocols approved by the University of Pittsburgh's Institutional Review Board. Electrode contacts that were identified as belonging to the seizure onset zone were not included in the analysis.

Patients were under the influence of different medications during the recording session depending on the stage of their visit at the epilepsy monitoring unit and their personal medical history. The medications typically consisted of various pain killers and anti-epileptic drugs. It is not possible for us to know which medications each individual was on at the exact time of the experimental sessions, due to insufficiencies in our notes during experimental sessions and insufficiencies in the medical records. The high level of heterogeneity in these medications may introduce sources of unmodeled cross-subject variance to the analyses (i.e., noise) that reduces statistical power, but are unlikely to introduce bias given their heterogeneity.

Electrodes were localized via postoperative CT scans or postoperative magnetic resonance images (MRI). Postoperative CT scans were co-registered to preoperative MRIs using Brainstorm.[57] Surface electrode contacts were projected to the nearest reconstructed cortical voxel of the preoperative MRI scan to correct for brain-shift.[58,59] These electrode locations were then registered to the Montreal Neurological Institute (MNI) common space via patient-specific linear interpolations.[60] VTC was defined as grey matter below the inferior temporal gyrus spanning from the posterior edge of the fusiform gyrus to the anterior temporal lobe in MNI common space. The main difference we observe between signals recorded from surface versus depth electrodes are small differences in the signal-to-noise ratio and spatial constraint of the signals, neither of which strongly influence the dynamics of the signals analyzes here.

Cortical distance between each electrode contact and the patient's occipital pole was computed using the patient's native neural anatomy. The occipital pole was defined as the intersection of the calcarine sulcus, inferior occipital gyrus, and superior occipital gyrus. The geodesic (cortical) distance between this point and the cortical surface coordinate nearest to each VTC electrode contact was computed using custom MATLAB scripts.[61]

METHOD DETAILS

Experimental paradigm

All patients underwent a category localizer task containing images occupying approximately 6° x 6° of visual angle at the center of a stimulus display monitor positioned 2 meters from the patient's eyes. Each stimulus was presented for 900 ms on a black background. Inter-stimulus intervals were 1500 ms with a random 0-400 ms jitter during which the patient saw a white fixation cross. Patients were instructed to press a button every time an image was presented twice in a row (1/6 of all trials). Repeat trials were excluded from further analysis. This left 70 trials per category to train and test the classifiers described in Multivariate temporal pattern analysis. Several patients underwent more than one run of this experiment and therefore had 140 or 210 trials per category. All experimental paradigms were presented via custom MATLAB scripts running the Psychophysics toolbox.[62]

35 patients underwent a category localizer task consisting of pictures of bodies, faces, hammers, houses, words, and non-objects. Six patients underwent category localizer tasks with slightly different object categories but with identical stimulus parameters. One of these patients viewed pictures of bodies, faces, *shoes*, hammers, houses, and phase-scrambled objects. One viewed pictures of bodies, faces, *consonant-strings*, *pseudowords*, real words, houses and phase-scrambled objects. One patient viewed pictures of faces, bodies, *consonant-strings*, words, hammers, and phase-scrambled objects. One viewed pictures of faces, bodies, words, *pseudowords*, houses, and phase-scrambled objects. One viewed pictures of faces, bodies, words, *tools*, *animals*, houses, and phase-scrambled objects. One viewed pictures of faces, bodies, words, *tools*, *animals*, *numbers*, houses, and phase-scrambled objects.

Intracranial recordings

Local field potentials were collected from iEEG electrodes via a GrapeVine Neural Interface (Ripple, LLC) sampling at 1 kHz. Notch filters at 60/120/180 Hz were applied online. Stimulus presentation was synchronized to the neural recordings via parallel port triggers sent from the stimulus displaying computer to the neural data acquisition computer. The signal was off-line filtered from 0.2-115 Hz using two-pass fourth order butter-worth filters via the FieldTrip toolbox.[63] In addition to analyzing these single trial potentials (stP), we also extracted and analyzed the single trial high frequency broadband (stHFBB) activity of these electrodes, since these two components of the local field potential have been shown to contain complimentary information[23,30] and may arise from different neurophysiological generators.[29]

StHFBB activity was extracted via Morlet wavelet decompositions from 70-150 Hz over 200 ms Hanning windows with 10 ms spacing. These specific frequency cutoffs were chosen due to their prevalence in human iEEG data analysis and the high cross-correlation of these response frequencies across different tasks and stimuli.[29,64,65] The resulting power spectral densities were then averaged over these frequency components and normalized to a baseline period from 500 ms to 50 ms prior to stimulus onset to yield the stHFBB activity. Data was then epoched from -500 to 1500 ms around stimulus presentation. Trials during which the stP amplitude changed more than 25 microvolts across a 1 ms sample, or during which stPs exceeded an absolute value greater than 350 microvolts, or during which either the stHFBB or stPs deviated more than 3 standard deviations from the mean were all assumed to contain noise and were therefore excluded.

Multivariate temporal pattern analysis

Related to Figures 1, 2, and S4. Sliding, leave-one-out cross-validated, Gaussian Naïve Bayes classifiers were applied to 100 ms time windows with 10 ms stride to determine if stHFBB or stP recorded from individual VTC contacts contained category-discriminant information. The input to these classifiers was 100 ms (100 samples) of stP and 100 ms (10 samples) of stHFBB from a single electrode contact. The output of the classifier was the category of object presented during the corresponding trial. This procedure was repeated for all VTC contacts from time windows beginning at 100 ms prior to stimulus onset to 1000 ms after stimulus onset.

The category-discriminant information content within each neural population was estimated by computing the mutual information ($I(S',S)$) between the output of the Gaussian Naïve Bayes classifiers (predicted category labels, S') for a given 100 ms time window of neural activity and the actual presented stimulus (S):

$$I(S',S) = P(S)\, log_2\left(\frac{P(S',S)}{P(S')P(S)}\right),$$

where $P(S',S)$ is the joint probability of the classifier correctly predicting the stimulus category S when the category was S, $P(S')$ is the proportion of times the classifier guessed a trial was of stimulus S, and $P(S)$ is the proportion of trials which the stimulus presented was S. This allowed us to estimate the category-discriminant information contained within 100 ms time windows without estimating a joint probability table of neural responses that was intractable.[66,67] It has been shown that this estimate of information, which relies on a $P(S',S)$ derived by an external classifier and not the actual neural code, is an underestimate of the neural information content.[68] Therefore, our calculated information is a lower bound for the actual neural information content.

Information content was averaged across all stimulus categories presented to the patient so as not to preclude electrode contacts as being selective for only one object category.[69] A threshold for significant category-discriminant information was determined by randomly shuffling stimulus labels for a subset of VTC electrode contacts and repeating the same classification analysis 1,000 times for each electrode contact.[70] Electrode contacts with the same number of runs of the category-localizer task demonstrated very similar null distributions and therefore we applied the result of this permutation test to all VTC electrode contacts. The threshold was chosen such that none of the random permutations

for any electrode contacts in the subset reached the threshold, which corresponds to $p < 0.001$, corrected for multiple temporal comparisons. Electrode contacts with peak category-discriminant neural information exceeding this threshold were defined as category-discriminant.

We performed a similar decoding analysis to determine the time-course of visual responses in individual electrode contacts (Figure S4). This was done by classifying single trial baseline periods (100 ms to 0 ms prestimulus presentation) of neural activity from these neural populations against sliding 100 ms time-windows from -90 to 1000 ms poststimulus presentation for all object categories treated as one class. This yielded a time-course of visual responses in each sampled neural population. By randomly permuting the label of the baseline versus evoked data and repeating the analysis in a subset of electrode contacts 1,000 times, we defined a threshold of visual information that no random permutation of the data achieved, corresponding to the $p < 0.001$, chance level, corrected for multiple temporal comparisons. We used this threshold to define visually responsive brain regions and those that were not, which were separated to calculate their differential contributions of functional connectivity to VTC electrode contacts with significant category-discriminant information (Figure 4).

Neural information processing dynamics

Related to Figures 2 and S4. To estimate properties of the information processing dynamics of neural populations across VTC, the information time-courses derived from the Naïve-Bayes classifiers were first smoothed with a running average filter (width 50 ms). Next, onset latency of category-discriminant information was defined as the last time point that an electrode contact was below 10 % of the maximum information prior to the peak information. The initial rise in category-discriminant information was defined as the time between the onset and the point where the information time-course first exceeded 90 % of the peak information. These cutoffs were chosen to ensure that small deviations from chance-level information and peak information did not affect the estimated quantities. Our main findings were robust to specific choices in threshold (Figure S8). Finally, we estimated the duration of information maintenance as the time between when the neural population first reached 90% of its peak information to when the neural population's information first fell below 50% of this maximum after peaking. Similar dynamic properties were also estimated for visual response time-courses (Figure S4) and information processing time-courses for specific object categories (Figure S5; Table S1).

Category-selective VTC electrode contacts

Related to Figure S5. To determine if neural populations with sensitivity to different object categories demonstrated differences in the gradients of their local dynamics or long-range functional connectivity, we isolated category-discriminant VTC neural populations that responded primarily to one object category. To do this we computed the event related potential and event related broadband responses to each category during the 1-back task. Next, any of the previously defined category-discriminant neural populations that contained maximum information to the same category that evoked the maximum response across either of these averages was classified as selective to that object category. We then characterized the information onset latency, slope, and connectivity of these neural populations using the procedures described above. For these analyses we used the category-specific information processing time-course derived from the Naïve Bayes classifiers prior to averaging over all categories in the main analysis.

Information processing simulations

Related to Figure S3. Simulations were used to test if increases in information processing duration exhibited along the ventral visual hierarchy could be explained by differences in peak information magnitude. Specifically, information time-courses were approximated as normal probability density functions (PDFs) parameterized by a mean, standard deviation, and magnitude (constant scaling). Normally distributed noise with the same standard deviation as prestimulus (-400 to 0 ms) information in category-selective VTC electrode contacts was then added to these curves. 1000 simulated signals were computed for each different PDF magnitude and standard deviation.

Information processing duration was calculated using the same procedure described for the actual signal, by calculating the time between when the signal first reached 90 % of its maximum amplitude and the last time it was below 10 % of its maximum before that. We then calculated the Spearman correlation between information processing duration when varying the PDF's standard deviation (to mimic changes in slope of the information processing time-course) and when varying the information's peak amplitude. Peak amplitude was varied from the minimum to maximum peak information in category-selective VTC electrode contacts. During the simulation investigating the effect of slope on information processing duration, signal amplitude was fixed at the average peak information in category-selective VTC electrode contacts.

Endogenous neural timescales

Related to Figure 3. The endogenous timescales of VTC populations were characterized by computing the autocorrelation of prestimulus (-500 ms to stimulus onset) stPs and prestimulus stHFBB activity from 1-250 ms lags during each clean trial of the 1-back task (i.e., those that were not excluded due to noise rejection criteria explained at the end of the section "Intracranial Recordings"). These prestimulus autocorrelation functions were then averaged over all trials. The average autocorrelation function for each electrode contact was then fit with a single exponential decay function:

$$ACF(t) = t_0 + N_0 e^{-t/\tau}$$

The neural timescale (tau), which measures the rate at which the autocorrelation function decays, was then correlated with several other functional properties of the neural population. This estimation of neural autocorrelations and computation of tau is similar to the procedure described in.[9]

Functional connectivity

Related to Figure 4. To determine the connectedness of VTC neural populations to the rest of the brain, phase-locking values (PLVs) were calculated between neural populations with above-chance levels of category-discriminant information and all other electrodes within the same patient (regardless of category-discriminant information content). Electrode contacts within 1 cm of the category-discriminant electrode were not included in the analysis to rule out effects caused purely by volume conduction. PLVs measure instantaneous phase-coupling across different brain regions independent of differences in amplitude, unlike coherence metrics.[71] This makes PLVs more sensitive to detecting weakly coupled oscillators despite differences in amplitude.[72] This coupling of oscillations is thought to indicate event-related communication between electrode contacts.

The instantaneous phase of each electrode contact during all category-localizer trials was computed via convolution of the filtered neural activity (from 1-115 Hz) with Morlet wavelets of frequencies ranging from 1-60 Hz (width = 5). This convolution allowed the separation of signal phase from envelope at each frequency.[73] Next, the PLV was computed by taking the vector average of the phase difference between two electrode contacts at each time point. PLVs close to 1 indicate two electrode contacts have similar phase differences at this frequency and time point across all trials. Conversely, if this number is close to 0, the phase difference between these electrode contacts is random at this given frequency and time point.

A spectral window of interest was defined to capture the part of the PLV spectrogram that showed increased functional connectivity across all category-discriminant VTC neural populations. We chose to focus on the time windows from -450 to 0 ms before stimulus onset to capture prestimulus functional connectivity of the neural populations. Next, we determined which frequency components demonstrated increased stimulus-evoked functional connectivity across VTC. To do this we averaged the PLVs from 50 to 500 ms and performed a paired t-test against the average PLV from -450 ms to 0 ms before stimulus presentation between the category-selective VTC electrode contacts and the rest of the electrode contacts in the same patient. This analysis revealed that frequency components between 1 and 22 Hz all had significantly greater phase-locking across all category-discriminant VTC electrode contacts relative to baseline on average from 50 to 500 ms after stimulus presentation ($p < 0.001$, corrected).

Therefore, we averaged the PLVs across electrode contacts from 2 to 22 Hz (discarding 1 Hz frequency band to increase the temporal precision of our estimated phase-locking), and -450 to 0 ms before stimulus onset to calculate the functional connectedness of these same regions. We separately averaged the connectivity of category-discriminant VTC neural populations with visually responsive regions (defined above) and those that were not visually responsive to determine if there were connectivity differences across these neural populations. Average functional connectivity from -450 to 0 ms prestimulus and 50-500 ms after stimulus presentation were strongly correlated with one another ($\rho = 0.96$, $p < 0.001$). Thus, results do not substantially change if either the prestimulus or post stimulus PLV is used.

Predicting response time from VTC activity

Related to Figure 5. To test for differences in the correlation between category-selective VTC population activity and behavior, patient RT was predicted using the neural activity from each category-selective contact. Specifically, a sliding window L2-regularized multiple regression (100 ms window, 10 ms stride) was used to predict patient RT from stP and stHFBB activity using a leave-one-trial-out cross-validation procedure. Only trials when the patient correctly reported that an object was repeated twice in a row were included in the analysis. The maximum Spearman correlation between the patient's RTs and the sliding-window RT predictions from 0-1000 ms after stimulus presentation was considered as the neural population's correlation with behavior. This correlation was then correlated with that population's dynamics, connectivity, and anatomical location.

QUANTIFICATION AND STATISTICAL ANALYSIS

Spearman rank-order correlations were used to calculate the correlations between anatomical position and aspects of the neural information time-courses calculated above. Spearman rank-order partial correlations were used to calculate the correlation between variables while correcting for correlations shared with other variables. Benjamini-Hochberg False Discovery Rate estimation which is valid for dependent hypothesis tests was used where noted.[74] Paired T-tests were used to determine if there were differences in the dynamics of processing different levels of information (visual versus category-discriminant) in the same electrode contacts.

Rank-order mixed-effects models were used to control for random effects of cross-patient variability while examining the main effects of connectivity and anatomical position on information processing dynamics. We chose to fit these mixed-effects models with equal slopes but random intercepts across patients to ensure the models converged. Because observations in mixed-effects models are not independent, it is difficult to determine the appropriate degrees of freedom. This makes estimation of *p*-values impossible without appropriate approximation. Therefore, to derive *p*-values for the main effects of the mixed-effects models, we use the Satterthwaite approximation, which has been shown to produce acceptable Type 1 error rates with relatively few samples.[75]

To examine differences in information processing dynamics across males and females, a separate set of linear mixed-effects models were fit to explain information processing as a function of distance along the visual hierarchy with an additional fixed effect of gender and an

interaction term of distance by gender. Participant identifier was included as a random effect to control for cross-patient variability. Gender did not have a significant effect ($p < 0.01$) on most of the neural dynamics studied in this paper.

Linear multiple regression models were used to compare gradients of information processing in VTC neural populations that were selective for different object categories. We only included the categories that most patients saw (bodies, words, faces, hammers, houses, and phase-scrambled objects). Specifically, linear models were used to predict information onset latency, peak magnitude, processing duration, maintenance duration, and connectedness as a function of the category-selective neural populations' distance from the occipital pole with an added factor indicating which category the neural population was selective for (Figure S5). Linear mixed-effects models were initially used for this analysis to simultaneously control for random effects across patients. However, these models failed to converge, likely indicating an insufficient number of data points per category and patient to estimate these random effects. Because face-selective electrode contacts were most prevalent in our population, we used this as our baseline and compared all other categories to face-selective electrode contacts (Table S1).